ADVANCED FUNCTIONAL MATERIALS
www.afm-journal.de

Fragile-to-Strong Transition in Phase-Change Material $Ge_3Sb_6Te_5$

Julian Pries, Hans Weber, Julia Benke-Jacob, Ivan Kaban, Shuai Wei, Matthias Wuttig,* and Pierre Lucas*

Chalcogenide phase-change materials combine a remarkable set of properties that makes them promising candidates for future non-volatile memory applications. Binary data storage exploits the high contrast in electrical and optical properties between the covalent amorphous and metavalent crystalline phase. Here the authors perform an analysis of the liquid phase kinetics of the phase-change material $Ge_3Sb_6Te_5$, which is the key to ultrafast switching speeds. By employing four experimental techniques, the viscosity is measured over sixteen orders of magnitude despite its propensity for fast crystallization. These measurements reveal that the liquid undergoes a transition in viscosity–temperature dependence associated with a liquid–liquid phase transition. The system exhibits a shallow viscosity change with temperature near the glass transition which stabilizes the memory cells in the amorphous state and which limits the severity of relaxation processes. Meanwhile, when heated during the writing process, the fragility increases to more than double, causing the viscosity to drop rapidly enabling a nanosecond crystallization speed. This change in viscosity–temperature dependence is highly unusual among glass forming liquids and is reminiscent of the behavior of water. This viscosity transition is also key to the technological success of phase-change materials for computer memory applications.

1. Introduction

Phase-change materials (PCMs) are attracting enormous interest for their application in high-density computer memories and artificial intelligence platforms based on neuromorphic computing.[1–3] The operation of PCMs entails switching between the crystalline and amorphous phases via the liquid phase. These three states of matter (crystal, glass, and liquid) each possess unique physical features that play a critical role in the operation of current and advanced PCM devices. The distinct physical properties of the amorphous and crystalline solid phase enable various schemes for encoding information in a robust non-volatile form,[4] while the rapid increase in viscosity with temperature of the undercooled liquid (UCL) phase enables fast crystallization.[5] Among these three phases the crystalline state has received the most attention and involves a chemical bonding type (namely metavalent bonding[6–11]) associated with a unique set of physical properties distinct from its metallic and covalent counterparts. Its high reflectivity and conductivity provide the necessary property contrast to the amorphous state for information storage and processing. The amorphous state has been less studied but exhibits a high intrinsic instability against temperature increase leading to remarkable behavior such as crystallization below its glass transition temperature T_g.[12,13] This phase is also technologically important due to its natural propensity for structural relaxation. This process leads to resistance drift and can limit applications such as multi-level data storage.[14–16] Finally, it was recently shown that the liquid phase of PCMs also exhibits unconventional physical features that are critical for the operation of memory devices.[5,17–21] Specifically, liquid PCMs appear to undergo a liquid–liquid phase transition (LLT) which is accompanied by a steep decrease in viscosity at temperatures in between T_g and the melting temperature T_m and a shallow viscosity at around T_g.[5,19] The steep decrease enables fast crystallization during the SET process (crystallization) due to the suddenly low viscosity above T_g. Also, the shallow viscosity temperature dependence near T_g stabilizes the glassy phase in the (amorphous) RESET state because the kinetic arrest takes places in the high-viscosity liquid state. Direct structural evidence for the presence of LLTs in liquid AIST (AgInSbTe) and $Ge_{15}Sb_{85}$ were recently presented by

J. Pries, J. Benke-Jacob, M. Wuttig
Institute of Physics IA
RWTH Aachen University
52074 Aachen, Germany
E-mail: pries@physik.rwth-aachen.de; wuttig@physik.rwth-aachen.de
H. Weber, I. Kaban
IFW Dresden
Institute of Complex Materials
01069 Dresden, Germany
S. Wei
Department of Chemistry and iMAT
Aarhus University
Aarhus-C DK-8000, Denmark
M. Wuttig
Peter Grünberg Institute (PGI 10)
Forschungszentrum Jülich
52428 Jülich, Germany
P. Lucas
Department of Materials Science and Engineering
University of Arizona
Tucson, AZ 85712, USA

The ORCID identification number(s) for the author(s) of this article can be found under https://doi.org/10.1002/adfm.202202714.

DOI: 10.1002/adfm.202202714

Zalden et al.[20] using femtosecond X-ray diffraction. A breakdown of the Stokes–Einstein relation near the melting point T_m of $Ge_1Sb_2Te_4$, $Ge_2Sb_2Te_5$, GeTe, AIST, and $Ge_{15}Sb_{85}$ was interpreted as resulting from the formation of locally favored structures and associated with the onset of an LLT as in the case of supercooled water.[17,18] But more importantly regarding PCM operation, these LLTs are commonly associated with a sudden change in viscosity–temperature dependence, referred to as a fragile-to-strong transition (FST)[5,19] according to the terminology developed by Angell to describe the viscosity–temperature dependence of glass-forming liquids.[22] Conventional liquids normally range from "strong" like silica, which exhibit an Arrhenius-like temperature dependence of viscosity, to "fragile" like o-terphenyl which exhibit a steep, super-Arrhenius temperature dependence of viscosity. However, the number of liquids, including water, that have been shown to undergo an unusual transition from fragile to strong is increasing.[23,24] This is the case of PCMs which are believed to universally undergo this type of FSTs.[5,19] But, as in the case of water, a direct observation of this viscosity transition in PCMs is precluded by fast crystallization in the temperature range called the "no-man's land" between T_g and T_m. Hence, a direct observation of viscosity data showing a FST for PCMs has so far remained elusive.

Here, we combine a set of four different experimental techniques involving calorimetry, electron microscopy, time-resolved reflectivity, and rheology to measure the temperature dependence of viscosity in a PCM nearly continuously over sixteen orders of magnitudes, spanning the entire range from below T_g to above the melting point T_m. All data sets are in excellent agreement and show that the viscosity of $Ge_3Sb_6Te_5$ is more than two times stronger at low temperature ($m \approx 40$) than at high temperature ($m \approx 100$), thereby providing unambiguous evidence for the presence of an FST in the $Ge_3Sb_6Te_5$ PCM.

2. Results

2.1. Differential Scanning Calorimetry

$Ge_3Sb_6Te_5$ exhibits the characteristic properties of PCMs such as high contrast in optical reflectivity and resistivity between the amorphous and crystalline form, see below and Figure S3, Supporting Information, respectively. While traditional PCMs crystallize below T_g at the standard heating rate[12,13,25] which is defined as ϑ_s = 20 °C min^{-1},[26] $Ge_3Sb_6Te_5$ exhibits a visible calorimetric glass transition prior to crystallization. This permits to unambiguously determine its standard glass transition temperature T_g = 193 °C (Figure S1, Supporting Information), which is obtained when a standard glass (formed upon cooling at ϑ_s from UCL) is reheated at ϑ_s. It also permits us to investigate the kinetics of the UCL as described in **Figure 1**. The heat capacity curves of amorphous $Ge_3Sb_6Te_5$ collected at various heating rates after cooling at the same rate from the undercooled liquid (above T_g but just before recrystallization) are shown in Figure 1a. The glass transition endotherm is visible before the crystallization exotherm occurs (revealed by the sudden drop in excess heat capacity). The endotherm is found to shift to a lower temperature with a lower heating rate, as the glass transition is a kinetic transition between the undercooled liquid and the glassy solid.[27] The ability to observe this transition is of much interest as it permits us to measure the activation energy for structural relaxation of the undercooled liquid that is commonly found to be equal to the activation energy for the shear viscosity near the glass transition.[27,28] This activation energy ΔH^* controls the shift in T_g with cooling rate ϑ and can therefore be extracted from the data of Figure 1a with the use of Equation (1):[26]

$$\vartheta = \vartheta_0 \exp\left[\frac{\Delta H^*}{RT_g}\right] \quad (1)$$

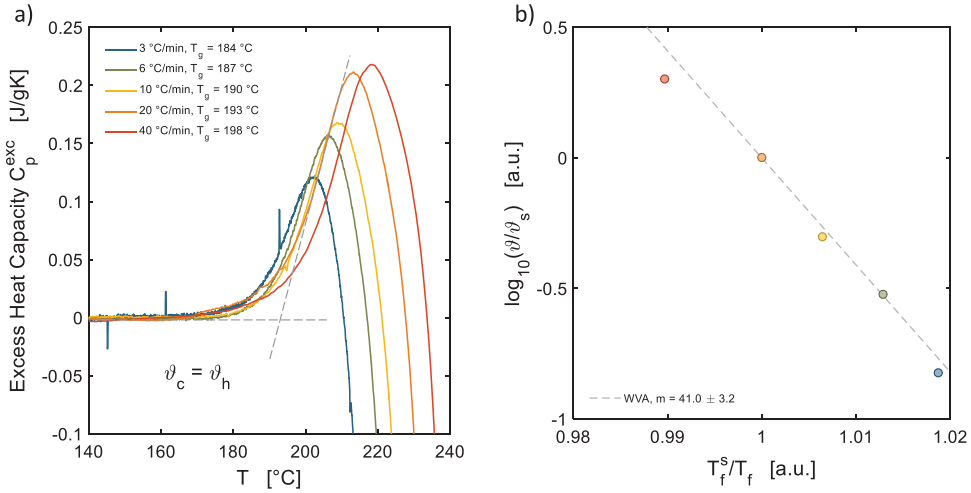

Figure 1. a) Excess heat capacity C_p^{exc} after initial vitrification from the undercooled liquid (UCL) during reheating at the same rate. Exothermic is down. The grey dash-dotted lines indicate the onset construction for obtaining the fictive temperature T_f. The resulting uncertainty on T_f is ≈1 °C, which amounts to an uncertainty on the fragility value of 3.2 including the fitting. b) Fictive temperature T_f as a function of cooling rate obtained from (a), where the cooling rate and subsequent heating rates are the same $\vartheta = \vartheta_c = \vartheta_h$. From fitting Equation (3) to the $T_f(\vartheta)$ data, the fragility close to the standard fictive temperature T_f^s is found to be equal to 41 from these DSC measurements.

where R is the gas constant and ϑ_0 is a constant.

Additionally, ΔH^* is related to the fragility parameter m according to Equation (2):[26]

$$m = \frac{\Delta H^*}{\ln(10)\mathrm{R}T_g} \tag{2}$$

so that a direct estimate of m can be obtained from ϑ and T_g using the construction shown in Figure 1b by fitting the Wang–Velikov–Angell (WVA) Equation (3):[26,29]

$$\log_{10}\left(\frac{\vartheta}{\vartheta_s}\right) = m\cdot\left(1-\frac{T_f^s}{T_f}\right) \tag{3}$$

where ϑ_s is the standard cooling rate of 20 °C min^{-1} and T_f is the fictive temperature. T_f describes the temperature where the structure or enthalpy of the glassy state and that of the UCL are identical.[30] The higher the cooling rate during vitrification, the higher the temperature where the glassy state departs from the UCL and thus the higher the T_f. Therefore, the fictive temperature T_f is a helpful quantity in describing and distinguishing glassy states. In the present case, the rate dependent T_f is found from the endothermic onset since the cooling and subsequent heating rate are identical.[28] Further the standard fictive temperature T_f^s is obtained at ϑ_s and thus is equal to T_g.

The results of Figure 1 reveal a relatively strong liquid behavior with $m = 41$, hence a rather mild change in viscosity with temperature is expected near T_g. In turn, the value of m derived this way permits to calculate the viscosity near T_g using the Mauro–Yue–Ellison–Gupta–Allan (MYEGA) equation,[31] based on the assumption that the shear viscosity is $\eta = 10^{12}$ Pa s at T_g. This allows a direct comparison to viscosity data obtained independently from crystal growth measurement utilizing electron microscopy and time-resolved reflectivity, as will be discussed in the next section.

2.2. Crystal Growth Measurements

Crystal growth in PCMs is limited by atomic diffusion through the undercooled liquid (UCL) such that the growth velocity v_g is proportional to the diffusion coefficient D according to:[32]

$$v_g(T) = \frac{8r_a}{\lambda^2}D(T)\left(1-\exp\left(-\frac{\Delta G(T)}{k_B T}\right)\right) \tag{4}$$

where λ is the interatomic jump distance, r_a is the atomic radius, and k_B is the Boltzmann constant. $\Delta G(T)$ is the Gibbs free energy difference between the crystal and the undercooled liquid which is approximated by the Thompson–Spaepen relation:[33]

$$\Delta G(T) = \Delta H_f\cdot\frac{T_m - T}{T_m}\cdot\frac{2T}{T_m + T} \tag{5}$$

where ΔH_f is the heat of fusion.

In principle, crystal growth velocity measurements can yield viscosity values, since the diffusion coefficient D and the viscosity η are inversely proportional according to the Stokes–Einstein relation (SER). However, Ediger et al.[34] have shown that the SER breaks down below ≈0.9 T_m, where diffusion is actually faster than expected from viscosity. The detailed origin of this decoupling is not clear at present but recent molecular dynamic simulations have suggested that crystal growth may be affected by nontrivial coupling between structural and compositional ordering.[35] In that temperature region the diffusion coefficient follows a relation of the form $D \propto \eta^{-\xi}$ where the exponent ξ ranges from 0 to 1 and depends linearly on the fragility index m.[34] Hence, for the undercooled liquid, the SER can be written as:

$$D = \left(\frac{k_B T}{6\pi R_{hyd}\eta}\right)^{\xi} \tag{6}$$

where R_{hyd} is the hydrodynamic radius (≈0.5 Å). Viscosity data can then be derived from crystal growth velocity measurements granted the fragility index m is known. In this work we follow an iterative process to obtain independent values for m and ξ from crystal growth velocity measurements. We first set $\xi = 1$ to obtain a set of viscosity values from v_g according to Equations (4) and (5). We then fit these data with the MYEGA equation using m and $\eta(T_g)$ as fitting parameters. The resulting m value is subsequently used to derive a new value of ξ using the relation derived by Ediger et al.[34] The process is repeated iteratively until the values of m and ξ have converged. This method was adopted because it permits us to obtain a set of viscosity data and a fragility parameter m that are independent from those derived by DSC. This allows for a more meaningful assessment of viscosity data derived calorimetrically and through crystal growth velocity. Below we employ two distinct techniques to measure the crystal growth velocity from which viscosity data is obtained.

2.3. Transmission Electron Microscopy

The first technique used to measure crystal growth velocity is based on time–temperature dependent imaging by transmission electron microscopy (TEM). Imaging is performed through a 30 nm thick $Ge_3Sb_6Te_5$ film encapsulated between two inert capping layers and deposited on a Si_3N_4 membrane serving as a TEM window (**Figure 2**a). The growth of a single crystalline grain is then monitored during an isothermal hold at temperatures ranging from 190 to 240 °C (Figure 2b). The crystal growth velocity v_g is found from the rate of the increasing grain radii. All temperatures are above the calorimetric T_g except for 190 °C. However, at that temperature, the measurements started after an equilibration time of 800 min. Considering that the relaxation time at T_g is ≈100 s, this ensures that all v_g measurements are performed in the undercooled liquid state. Furthermore, when the temperature is increased from 190 to 240 °C, the number of grains formed per area decreases. Hence judging from the grain size, $Ge_3Sb_6Te_5$ is a growth-dominated material especially at high temperatures, see Figure S4, Supporting Information.

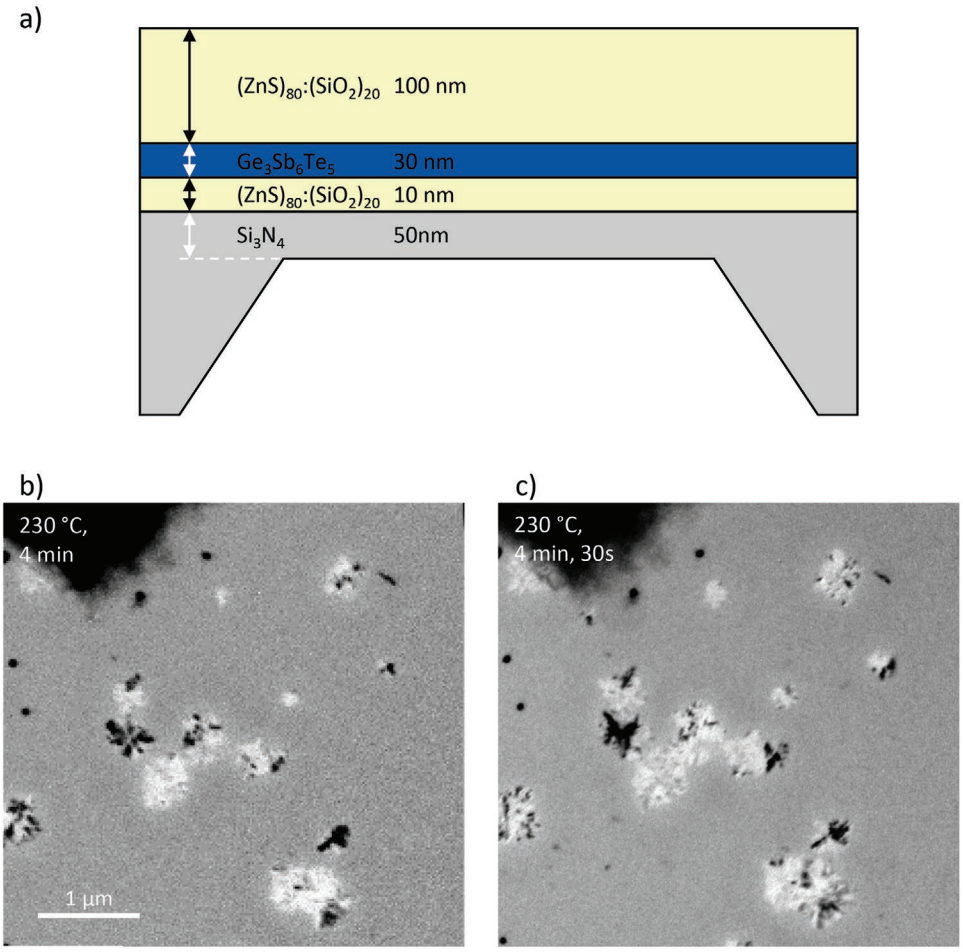

Figure 2. a) In-plane schematic of TEM sample (layer stack) for time–temperature dependent crystal growth velocity imaging. b,c) TEM images of grain growth in a $Ge_3Sb_6Te_5$ film during isothermal hold at 230 °C.

2.4. Time-Resolved Reflectivity

The second technique used to measure the crystal growth velocity v_g takes advantage of the large contrast in reflectivity between the crystalline and amorphous phase of PCMs, similar to the technique described in Ref. [32]. The growth velocity is monitored through the change in reflectivity of a $Ge_3Sb_6Te_5$ film during crystallization at a set temperature. The reflected intensity is proportional to the crystallized area and since the crystallization of $Ge_3Sb_6Te_5$ is growth-dominated, the rate of change in the reflectivity provides a direct measure of v_g. The experimental set-up of this phase-change optical tester (POT) is composed of a low-intensity continuous wave (CW) laser operating at a wavelength λ of 639 nm and a pulsed laser (λ = 658 nm) overlapping on the surface of the crystalline $Ge_3Sb_6Te_5$ film. The crystallized film is first melted locally (the resulting amorphous spot diameter is ≈1.5 µm) with a 30 ns laser pulse while the detected change in reflectivity of the layer stack is monitored with the CW laser as shown in **Figure 3**. This technique permits us to measure rapid growth provided that the crystallization time is longer that the pulsed thermalization time which is estimated to be ≈100 ns. In the present work, the crystal growth velocity v_g could be measured from 250 to 400 °C. Please note, that the deposited layers of the samples that are shown in Figure 2a used for POT and TEM crystallization measurements are identical and were prepared in the same magnetron sputter deposition run to ensure comparability. The only difference between the TEM and POT samples is that in the TEM samples, the silicon substrate is mechanically and chemically removed to allow for the permeability of electrons through the layers in TEM. In POT samples, the silicon substrate situated under the Si_3N_4 layer dissipates the heat of the laser well, preventing damage to the sample.

The crystal growth velocity measurements obtained by TEM and POT from 190 to 400 °C are shown in **Figure 4**a. The two set of measurements are in excellent agreement and show a nearly perfect Arrhenius dependence with temperature. The corresponding viscosity values are calculated according to Equations (4) and (5) following the iterative procedure described above. Fitting the TEM data with the MYEGA equation yields a fragility parameter m = 38.6 and a decoupling parameter ξ = 0.91. This value of m is in good agreement with that obtained by DSC (m = 41). The viscosity values obtained by crystal growth are compared with that derived from DSC using the MYEGA equation for temperatures of 184, 187, 190, 193, and 198 °C. Figure 4b shows that viscosity data derived by calorimetry are

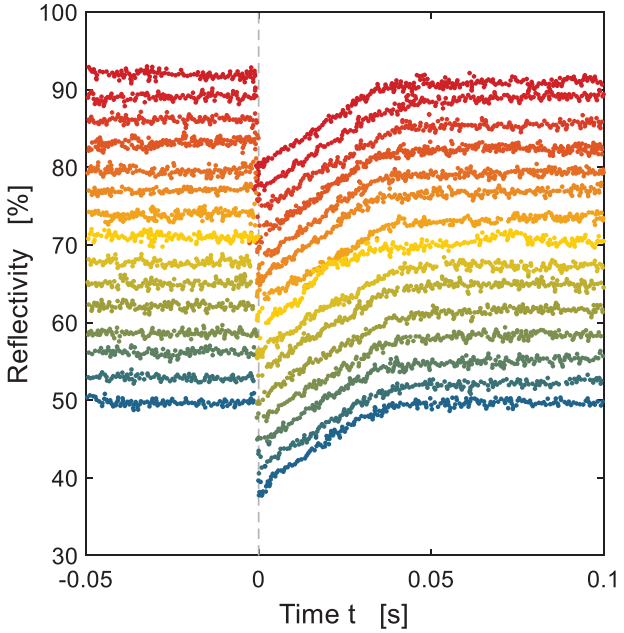

Figure 3. Time-resolved reflectivity measurement during recrystallization using the POT setup at 300 °C. At $t = 0$ s, an amorphous mark is induced into the crystalline matrix by laser-assisted melt-quenching which leads to a sudden decrease in the detected reflectivity of the sample. Upon recrystallization, the reflectivity increases again until it reaches a plateau when crystallization is completed. Here at 300 °C, it takes ≈0.0395 s for crystallization to complete. The radius of the amorphous mark is 0.75 µm. This results in a crystal growth velocity of 19 µm s^{-1}. To allow for distinguishing individual measurements the measurements are shifted by a value of 3 with respect to the previous measurement (blue data is not shifted).

in good agreement with that derived from crystal growth. The viscosity value obtained from TEM at the calorimetric T_g is $\eta = 10^{12.36}$ Pa s, which is comparable to the value $\eta = 10^{12}$ Pa s applied for calculating the viscosity from DSC.

2.5. Oscillating-Cup Viscometry

While the viscosity data shown in Figure 4b range over 12 orders of magnitude, high temperature viscosity data above T_m are also necessary to evaluate the fragility of $Ge_3Sb_6Te_5$ melt in the low viscosity regime. The method of choice for measuring viscosity at high temperature is oscillating-cup viscometry (OCV).[36] It has been broadly used to measure the viscosity of molten metallic alloys[36–38] as well as chalcogenide melts, including PCMs.[39–42] Viscosity data obtained by OCV have been validated by other methods and are found to be in excellent quantitative agreement with viscosities measured by electrostatic levitation as shown in Figure S5, Supporting Information.[43] Overall, the statistical uncertainty of OCV is found to be 5–10%.[36]

Viscosity data for the $Ge_3Sb_6Te_5$ melt ranging from 568 to 981 °C are shown on **Figure 5**a. Data points below the melting temperature T_m = 575 °C first overshoot then collapse due to the nucleation and growth of crystallites. Fitting the data points above T_m with the MYEGA equation yields a fragility index $m = 100.9$ as shown in Figure 5b. This value of m is more than twice larger than that measured near T_g by DSC and TEM ($m \approx 40$), thereby providing evidence for the presence of an FST in the PCM $Ge_3Sb_6Te_5$. In Figure 5b, the logarithmic plot combining viscosity data from all four methods shows that a sudden change in fragility must occur just below T_m in order to reconcile all data sets. A linear extrapolation of the low temperature data obtained by DSC, TEM, and POT would yield an unphysically small viscosity limit $\eta_\infty \approx 10^{-28}$ Pa s at high temperature. This crisis is averted by the occurrence of the LLT slightly below T_m which gives rise to the change in fragility.

3. Discussion

The first observation of an FST was reported by Ito et al. in water.[23] Since then, many glass forming liquids have been shown to exhibit viscous behavior consistent with FSTs,

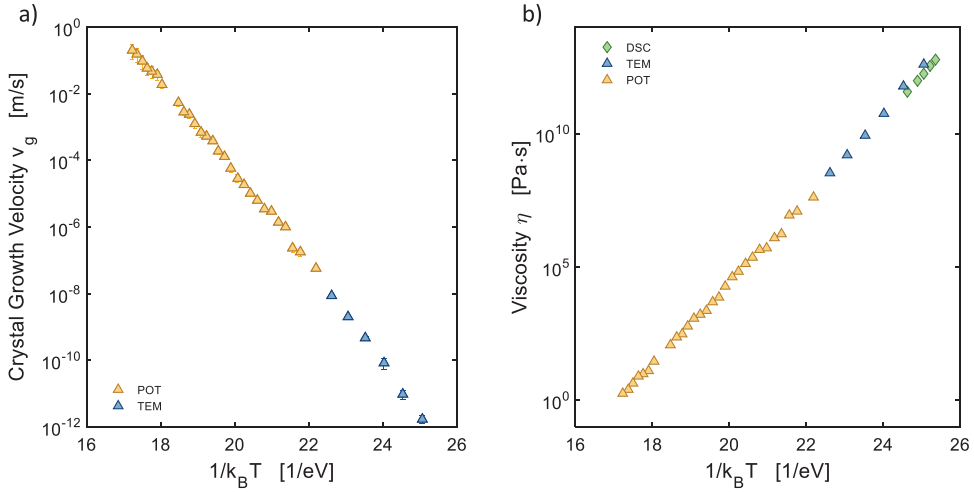

Figure 4. a) Combined data on crystal growth velocity v_g as measured from transmission electron microscopy (TEM) and by the laser setup of the phase change optical setup (POT). The uncertainty on the crystal growth velocity in TEM and POT measurements is ≈10% of the nominal value. b) Viscosity η calculated from the crystal growth velocity v_g as described in the main text. The viscosity data obtained through crystal growth measurements are in excellent agreement with that derived from DSC.

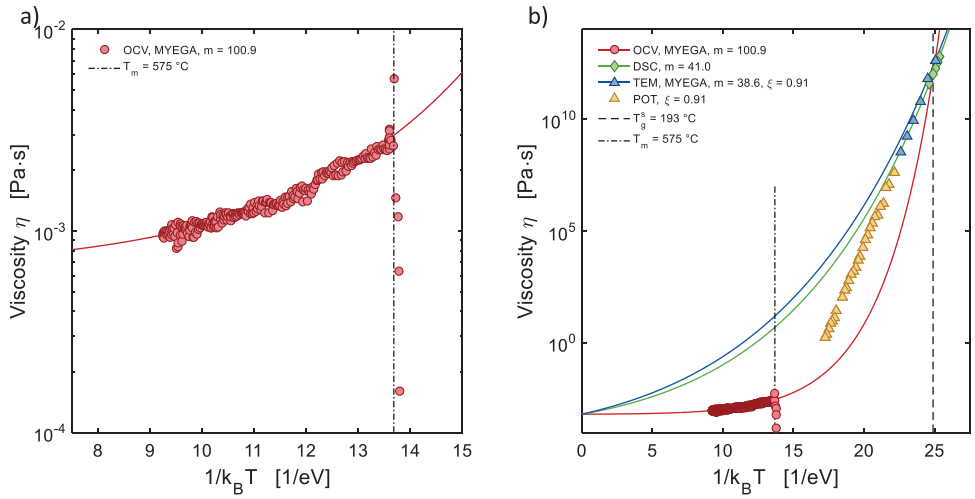

Figure 5. a) Viscosity of $Ge_3Sb_6Te_5$ melt measured by oscillating-cup viscometry (OCV). b) Logarithmic plot of viscosity data obtained over the entire temperature range from 184 to 981 °C using DSC, TEM, POT, and OCV.

especially metallic liquids[38,44] and chalcogenide melts.[19,45] However, these systems tend to be poor glass-formers, so that fast crystallization usually prevents a direct observation of the full FST. This is largely the case of telluride melts such as PCMs with the exception of $Ge_{15}Te_{85}$. This material can be supercooled slightly below its eutectic temperature and reveals the onset of a divergence in viscosity as shown in the Angell-plot of **Figure 6**[42,45] where viscosity data are plotted as a function of inverse temperature scaled by T_g. Interestingly, when plotted in this fashion, the viscosity data of $Ge_{15}Te_{85}$ overlap almost perfectly with those of $Ge_3Sb_6Te_5$ as well as those of the PCM AIST (those data points are almost entirely hidden behind those of $Ge_3Sb_6Te_5$). These tellurides data also overlap well with those of pure tellurium. This suggests that the atomic transport mechanism controlling viscous flow in each system must be very similar as they all tend to the same high-temperature viscosity limit of $\eta_\infty \approx 10^{-3.18}$ Pa s, as found for $Ge_3Sb_6Te_5$. However, contrary to a material that can be described by a single fragility m value like GeO_2 or OTP, a MYEGA fit of the high temperature data for $Ge_3Sb_6Te_5$ shows a dramatic mismatch with the low temperature viscosity. The viscosity of $Ge_3Sb_6Te_5$ must at some point undergo a divergence to reconnect with the low fragility data closer to T_g. Interestingly, the divergence experienced by $Ge_{15}Te_{85}$ offers a credible path through which the two data sets for $Ge_3Sb_6Te_5$ could be reconciled. Unfortunately, in $Ge_3Sb_6Te_5$ measurements below the melting temperature are not possible due to fast crystallization, but the similarity in behavior of $Ge_3Sb_6Te_5$ and $Ge_{15}Te_{85}$ at high temperature supports the suggestion that the two systems would exhibit an LLT. However, there is no evidence that all PCM should undergo an FST in the same reduced temperature range. Nevertheless AIST is also found to undergo an LLT in a similar range near $T_g/T \approx 0.67$.[20] The almost perfect Arrhenius behavior in $Ge_3Sb_6Te_5$ of the low temperature viscosity is unusual but is actually very similar to that of BeF_2 whose anomalous behavior was pointed out long ago by Angell.[46] Molecular dynamic simulations of the high temperature liquid later showed that BeF_2 indeed undergoes an FST like several other tetrahedral liquids including water.[47,48] In this light, the viscosity data collected for $Ge_3Sb_6Te_5$ are consistent with and in favor of the presence of an FST.

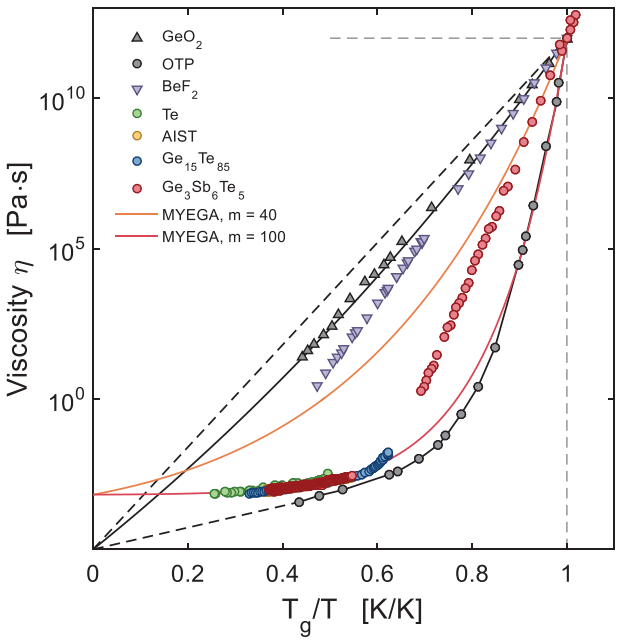

Figure 6. Fragility plot comparing the viscosity behavior of $Ge_3Sb_6Te_5$ melt with that of the standard strong liquid GeO_2[24] and standard fragile liquid o-terphenyl (OTP)[45] as well as Te,[49] several PCMs[42,50] and the tetrahedral liquid BeF_2.[51,52]

It is also worth noting that the LLTs believed to be responsible for the FST observed in multiple chalcogenide melts are also revealed by sharp anomalies in several thermodynamic functions.[5,19,24,53] For example, $Ge_{15}Te_{85}$ exhibits a sharp extremum in heat capacity, thermal expansion coefficient, and adiabatic compressibility at the same temperature as the viscosity divergence.[24,53,54] This behavior is observed in multiple other chalcogenide melts.[19] A correlation between the dynamic and thermodynamic properties of liquids is indeed expected from the Adam–Gibbs equation which relates the kinetics of glass-forming liquids to their configurational entropy.[55] Martinez

and Angell also established a universal correlation between the temperature dependence of the viscosity and the configurational entropy of glass-forming liquids encompassing the full range of fragility.[56] In the case of $Ge_{15}Te_{85}$, a quantitative correlation was established between the thermodynamic anomaly at the LLT and the viscosity divergence at the FST.[45] These LLTs are also commonly associated with a semiconductor-to-metal transition and a negative expansion coefficient.[5,19,57,58] This semiconductor-to-metal transition is believed to be essential in determining the success of PCMs as non-volatile memory materials.[5] But the FST itself is also key for PCM operation as it affects the switching speed and stability of the memory cells as follows.

Relaxation dynamics differ for strong and fragile glass forming liquids. The higher the fragility, the more structural relaxation the system will experience while in the glassy state (RESET state).[59] This is detrimental as pronounced relaxation processes lead to pronounced aging effects like density increase and resistivity drift.[14] Small temperature changes also lead to a large change in relaxation time in fragile systems, thereby leading to the potential instability of the glassy memory cell upon temperature variations. Hence it is beneficial for the system to exhibit a strong character in the low temperature regime near T_g. On the other hand, switching speed is enhanced by low viscosity so that high fragility is desirable when the temperature is increased in between T_g and the melting point for the SET process. The transition from strong to fragile upon heating therefore provides the benefit of speed while retaining the amorphous cell stability. As shown in Figure 6, the viscosity near a desirable SET temperature ($T_g/T \approx 0.6$) would be nearly four orders of magnitude higher if the system remained strong. In turn, the crystal growth velocity v_g and consequently the switching speed would be four orders of magnitude slower. Figure 6 then provides directions for optimizing the SET temperature with the goal of maximizing speed while minimizing power. In addition, $Ge_3Sb_6Te_5$ is growth-dominated so that scaling down the memory cell radius would increase switching speed while decreasing energy consumption due to the smaller volume of material being heated.

A parameter that has proven useful in describing the amorphous phase stability against crystallization is the reduced glass transition temperature $T_{rg} = T_g/T_m$.[60] The value for $Ge_3Sb_6Te_5$ of 0.55 is indeed higher than that of the prototypical PCMs $Ge_2Sb_2Te_5$; 0.52[12] or GeTe; 0.46.[25] While other PCMs crystallize from the glassy phase, the glass transition in $Ge_3Sb_6Te_5$ can be observed, see Figure 1, which further underlines its increased amorphous phase stability. We performed additional minimum crystallization time measurements similar to Ref. [11] which indicates the minimum time to crystallize a completely amorphous PCM film at optimal conditions. This measurement resulted in a value of ≈50 ns, see Figure S6, Supporting Information. This value is smaller than that of $Ge_2Sb_2Te_5$; 80 nm and GeTe; 600 ns reported in Ref. [11] and hence indicates advantageous crystallization kinetics. It must be noted, that these values include the period of crystal nucleation, namely the time until the first grain forms. This is contrary to the situation in memory devices where a significant fraction of the cell is crystallized directly from the crystalline surrounding. Thus, crystallization in a device will be faster than those numbers suggest. Nevertheless, this result shows that $Ge_3Sb_6Te_5$ offers the fastest crystallization speeds.

4. Conclusion

LLTs and FSTs have received much attention in the last two decades, in particular due to their presence in the most essential of liquids: water. While it has been observed in an increasing number of other systems, it has mainly raised interest as a fundamental scientific challenge. Here we show that these FSTs also play a key technological role in enabling the application of phase-change materials in non-volatile memory devices. The dramatic change in liquid kinetics associated with the FST enables the combination of ultrafast crystallization at high temperature and maximum glassy state stability at low temperature, which would not be achievable in glass-forming liquids obeying a conventional single fragility behavior. While the data provided in this study are limited to the $Ge_3Sb_6Te_5$ composition, LLTs have been observed in a number of other chalcogenides systems[5,20] and it is expected that FSTs are a universal feature of chalcogenide PCMs. However, further techniques are required to elucidate the mechanism responsible for the FST. The cell stability afforded by the strong behavior near T_g is also particularly relevant for the development of neuromorphic computing[3] and multi-level data storage[14] where even small structural relaxation leads to significant resistance drift. This change in resistance leads to read-out errors of encoded levels in multi-level data storage or drift of the emulated synaptic weight in neuromorphic devices. Further investigation of the material's "strong" behavior near T_g could therefore have significant technological implications. Therefore, we can conclude that $Ge_3Sb_6Te_5$ exhibits an FST that affords the excellent and advantageous PCM-characteristics.

5. Experimental Section

Powders for calorimetric measurements of $Ge_3Sb_6Te_5$ were prepared from a stoichiometric target by magnetron sputter deposition at a base pressure of 3×10^{-6} mbar. The composition and film thickness were measured in a Scanning Electron Microscope (SEM) of FEI Helios Dual Beam FIB and the results are given in the Supporting Information.

For measuring the crystal growth velocity of $Ge_3Sb_6Te_5$, the authors adopted the layer system described in Ref. [32] which was also prepared by magnetron sputter deposition. This layer system allowed for the preparation of TEM samples by mechanical polishing and chemical etching. Moreover, utilizing this layer stack enabled the measurement of the crystal growth velocity from samples that were prepared in the same sputtering deposition process with both techniques, that is, TEM and the laser setup of the POT. This way a maximum of comparability was ensured.

The excess heat capacity C_p^{exc} data was measured in a PerkinElmer Diamond DSC. The measured temperature at a constant heating rate ϑ was calibrated by the onset of melting of pure indium as already reported in the Supporting Information of Ref. [12]. The excess heat capacity $C_p^{exc}(T)$ is obtained from subtracting the rescan of the crystallized material taken subsequently to the initial measurement.

All TEM measurements were performed on a FEI Tecnai F20 in energy filtered bright field mode. The samples were heated at a distinct temperature for a certain time interval in the DSC which served as a precise oven. After the heat treatment, formed crystalline grains were identified and photographed in TEM. The heating and TEM imaging was

repeated until the same grains were photographed at least three times. From the grain size, the radius was measured and its change with time, the crystal growth velocity, was determined.

In POT measurements of crystal growth velocity, the sample was initially crystallized. Afterwards, the sample stage was heated to a constant temperature at which the crystal growth velocity ought to be measured. When isothermal conditions were reached, a region of 1.5 µm in diameter was amorphized by a melt-quenching laser pulse while the reflectivity was probed. From the change in reflectivity, the change in radius is inferred which yields the crystal growth velocity.

The oscillating-cup viscometry (OCV) method was used to measure the viscosity of $Ge_3Sb_6Te_5$. The elements were weight out and sealed in a quartz ampoule, which was previously flooded with argon gas at a remaining pressure of 0.25 bar.

Statistical Analysis: Power data taken by DSC was converted to specific heat capacity in Pyris Series Software by PerkinElmer and was further analyzed in a self-developed program in Matlab by Mathworks including the determination of the endothermic onset and the fragility fitting depicted in Figure 1. The uncertainty of the onset temperature was about ±1 °C.

In TEM, nucleated and growing grains were observed directly. Grains grow in a circular fashion and therefore the grain radius was found from the smallest circle that contained the whole grain. Circles were placed around the grains and the radius was elaborated in DigitalMicrograph by Gatan. At every temperature at least six grains (up to 21) were investigated over three annealing steps. The crystal growth velocity was found from the change in radius with time in a self-developed Matlab program. Also, in Matlab was done the calculation of the viscosity from the crystal growth velocity data of TEM and POT samples. The uncertainty of the TEM measurements is estimated from the size of the pixels in the image and how accurate a circle can be placed around the grains. For every temperature the crystal growth velocity of the individual grains is averaged and the experimental error is combined with the statistical scatter. The overall error on the crystal growth velocity amounted to ≈10% of the nominal (mean) value.

In POT, at every temperature at least ten measurements were conducted. The time for recrystallization was obtained for each measurement and averaged in a self-developed Matlab program. The laser setup was operated by a self-designed LabView script. The averaging resulted in values for the mean and the standard deviation. The scatter in the recrystallization interval was the dominant cause of uncertainty of the obtained experimental values. It also amounted to ≈10% of the nominal (mean) crystal growth velocity value.

Supporting Information

Supporting Information is available from the Wiley Online Library or from the author.

Acknowledgements

The authors acknowledge funding from the Deutsche Forschungsgemeinschaft (DFG) via the collaborative research center Nanoswitches (SFB 917). PL acknowledges funding from NSF-DMR grant#: 1832817.

Open access funding enabled and organized by Projekt DEAL.

Conflict of Interest

The authors declare no conflict of interest.

Data Availability Statement

The data that support the findings of this study are available from the corresponding author upon reasonable request.

Keywords

crystallization kinetics, fragile-to-strong transitions, liquid-liquid transitions, phase-change materials, undercooled liquids

Received: March 8, 2022
Revised: April 20, 2022
Published online: May 12, 2022

[1] W. Zhang, R. Mazzarello, M. Wuttig, E. Ma, *Nat. Rev. Mater.* **2019**, *4*, 150.
[2] J. Feldmann, N. Youngblood, M. Karpov, H. Gehring, X. Li, M. Stappers, M. Le Gallo, X. Fu, A. Lukashchuk, A. S. Raja, J. Liu, C. D. Wright, A. Sebastian, T. J. Kippenberg, W. H. P. Pernice, H. Bhaskaran, *Nature* **2021**, *589*, 52.
[3] M. Xu, X. Mai, J. Lin, W. Zhang, Y. Li, Y. He, H. Tong, X. Hou, P. Zhou, X. Miao, *Adv. Funct. Mater.* **2020**, *30*, 2003419.
[4] M. Wuttig, N. Yamada, *Nat. Mater.* **2007**, *6*, 824.
[5] S. Wei, P. Lucas, C. A. Angell, *MRS Bull.* **2019**, *44*, 691.
[6] J.-Y. Raty, M. Schumacher, P. Golub, V. L. Deringer, C. Gatti, M. Wuttig, *Adv. Mater.* **2019**, *31*, 1806280.
[7] M. Wuttig, V. L. Deringer, X. Gonze, C. Bichara, J.-Y. Raty, *Adv. Mater.* **2018**, *30*, 1803777.
[8] B. J. Kooi, M. Wuttig, *Adv. Mater.* **2020**, *32*, 1908302.
[9] M. Zhu, O. Cojocaru-Mirédin, A. M. Mio, J. Keutgen, M. Küpers, Y. Yu, J.-Y. Cho, R. Dronskowski, M. Wuttig, *Adv. Mater.* **2018**, *30*, 1706735.
[10] L. Guarneri, S. Jakobs, A. von Hoegen, S. Maier, M. Xu, M. Zhu, S. Wahl, C. Teichrib, Y. Zhou, O. Cojocaru-Mirédin, M. Raghuwanshi, C.-F. Schön, M. Drögeler, C. Stampfer, R. P. S. M. Lobo, A. Piarristeguy, A. Pradel, J.-Y. Raty, M. Wuttig, *Adv. Mater.* **2021**, *33*, 2102356.
[11] C. Persch, M. J. Müller, A. Yadav, J. Pries, N. Honné, P. Kerres, S. Wei, H. Tanaka, P. Fantini, E. Varesi, F. Pellizzer, M. Wuttig, *Nat. Commun.* **2021**, *12*, 4978.
[12] J. Pries, S. Wei, M. Wuttig, P. Lucas, *Adv. Mater.* **2019**, *31*, 1900784.
[13] J. Pries, J. C. Sehringer, S. Wei, P. Lucas, M. Wuttig, *Materials Science in Semiconductor Processing 2021*, Vol. *134*, p. 105990.
[14] W. Zhang, E. Ma, *Mater. Today* **2020**, *41*, 156.
[15] J. Y. Raty, W. Zhang, J. Luckas, C. Chen, R. Mazzarello, C. Bichara, M. Wuttig, *Nat. Commun.* **2015**, *6*, 7467.
[16] S. Gabardi, S. Caravati, G. C. Sosso, J. Behler, M. Bernasconi, *Phys. Rev. B: Condens. Matter Mater. Phys.* **2015**, *92*, 054201.
[17] S. Wei, Z. Evenson, M. Stolpe, P. Lucas, C. A. Angell, *Sci. Adv.* **2018**, *4*, 8632.
[18] S. Wei, C. Persch, M. Stolpe, Z. Evenson, G. Coleman, P. Lucas, M. Wuttig, *Acta Mater.* **2020**, *195*, 491.
[19] P. Lucas, S. Wei, C. A. Angell, *Int. J. Appl. Glass Sci.* **2020**, *11*, 236.
[20] P. Zalden, F. Quirin, M. Schumacher, J. Siegel, S. Wei, A. Koc, M. Nicoul, M. Trigo, P. Andreasson, H. Enquist, M. J. Shu, T. Pardini, M. Chollet, D. Zhu, H. Lemke, I. Ronneberger, J. Larsson, A. M. Lindenberg, H. E. Fischer, S. Hau-Riege, D. A. Reis, R. Mazzarello, M. Wuttig, K. Sokolowski-Tinten, *Science* **2019**, *364*, 1062.
[21] J. Orava, D. W. Hewak, A. L. Greer, *Adv. Funct. Mater.* **2015**, *25*, 4851.
[22] C. A. Angell, *J. Non-Cryst. Solids* **1991**, *133*, 13.
[23] K. Ito, C. T. Moynihan, C. A. Angell, *Nature* **1999**, *398*, 492.
[24] P. Lucas, *J. Non-Cryst. Solids: X* **2019**, *4*, 100034.
[25] J. Pries, Y. Yu, P. Kerres, M. Häser, S. Steinberg, F. Gladisch, S. Wei, P. Lucas, M. Wuttig, *Phys. Status Solidi RRL* **2021**, *15*, 2000478.
[26] L.-M. Wang, V. Velikov, C. A. Angell, *J. Chem. Phys.* **2002**, *117*, 10184.
[27] C. T. Moynihan, *Rev. Miner.* **1995**, *32*, 1.

[28] C. T. Moynihan, S. K. Lee, M. Tatsumisago, T. Minami, *Thermochim. Acta* **1996**, *280*, 153.
[29] J. Pries, S. Wei, F. Hoff, P. Lucas, M. Wuttig, *Scr. Mater.* **2020**, *178*, 223.
[30] A. Q. Tool, *J. Res. Natl. Bur. Stand. (U. S.)* **1945**, *34*, 199.
[31] J. C. Mauro, Y. Yue, A. J. Ellison, P. K. Gupta, D. C. Allan, *Proc. Natl. Acad. Sci. USA* **2009**, *106*, 19780.
[32] M. Salinga, E. Carria, A. Kaldenbach, M. Bornhofft, J. Benke, J. Mayer, M. Wuttig, *Nat. Commun.* **2013**, *4*, 2371.
[33] C. V. Thompson, F. Spaepen, *Acta Metall.* **1979**, *27*, 1855.
[34] M. D. Ediger, P. Harrowell, L. Yu, *J. Chem. Phys.* **2008**, *128*, 034709.
[35] Y.-C. Hu, H. Tanaka, *Sci. Adv.* **2020**, *6*, eabd2928.
[36] S. Gruner, W. Hoyer, *J. Alloys Compd.* **2009**, *480*, 629.
[37] C. Zhou, L. Hu, Q. Sun, H. Zheng, C. Zhang, Y. Yue, *J. Chem. Phys.* **2015**, *142*, 064508.
[38] C. Zhang, L. Hu, Y. Yue, J. C. Mauro, *J. Chem. Phys.* **2010**, *133*, 014508.
[39] V. M. Glazov, O. V. Situlina, *Dokl. Akad. Nauk SSSR* **1969**, *187*, 799.
[40] A. Laugier, G. Chaussemy, J. Fornazero, *J. Non-Cryst. Solids* **1977**, *23*, 419.
[41] M. Schumacher, H. Weber, P. Jovari, Y. Tsuchiya, T. G. A. Youngs, I. Kaban, R. Mazzarello, *Sci. Rep.* **2016**, *6*, 27434.
[42] H. Weber, J. Orava, I. Kaban, J. Pries, A. L. Greer, *Phys. Rev. Mater.* **2018**, *2*, 093405.
[43] D. C. Van Hoesen, A. K. Gangopadhyay, G. Lohöfer, M. E. Sellers, C. E. Pueblo, S. Koch, P. K. Galenko, K. F. Kelton, *Phys. Rev. Lett.* **2019**, *123*, 226601.
[44] C. Way, P. Wadhwa, R. Busch, *Acta Mater.* **2007**, *55*, 2977.
[45] S. Wei, P. Lucas, C. A. Angell, *J. Appl. Phys.* **2015**, *118*, 034903.
[46] C. A. Angell, *J. Non-Cryst. Solids* **1985**, *73*, 1.
[47] M. Hemmati, C. T. Moynihan, C. A. Angell, *J. Chem. Phys.* **2001**, *115*, 6663.
[48] C. A. Angell, R. D. Bressel, M. Hemmati, E. J. Sare, J. C. Tucker, *Phys. Chem. Chem. Phys.* **2000**, *2*, 1559.
[49] V. M. Glazov, O. D. Shchelikov, *Izv. Akad. Nauk SSSR, Neorg. Mater.* **1974**, *10*, 202.
[50] J. Orava, H. Weber, I. Kaban, A. L. Greer, *J. Chem. Phys.* **2016**, *144*, 194503.
[51] S. V. Nemilov, G. T. Petrovskii, L. A. Krylova, *Izv. Akad. Nauk SSSR, Neorg. Mater.* **1968**, *4*, 1664.
[52] C. T. Moynihan, S. Cantor, *J. Chem. Phys.* **1968**, *48*, 115.
[53] Y. S. Tver'yanovich, V. L. Ugolkov, O. V. Il'chenko, *J. Non-Cryst. Solids* **1999**, *257*, 78.
[54] Y. S. Tver'yanovich, V. L. Ugolkov, *NATO Sci. Ser. II* **2002**, *81*, 209.
[55] G. Adam, J. H. Gibbs, *J. Chem. Phys.* **1965**, *43*, 139.
[56] L. M. Martinez, C. A. Angell, *Nature (London, U. K.)* **2001**, *410*, 663.
[57] S. Wei, G. J. Coleman, P. Lucas, C. A. Angell, *Phys. Rev. Appl.* **2017**, *7*, 034035.
[58] M. Cobelli, D. Dragoni, S. Caravati, M. Bernasconi, *Phys. Rev. Mater.* **2021**, *5*, 045004.
[59] E. A. King, S. Sen, W. Takeda, C. Boussard-Pledel, B. Bureau, J.-P. Guin, P. Lucas, *J. Chem. Phys.* **2021**, *154*, 164502.
[60] D. Turnbull, *Contemp. Phys.* **1969**, *10*, 473.